

Aligning Partially Overlapping Point Sets: an Inner Approximation Algorithm

Wei Lian, Wangmeng Zuo and Lei Zhang

Abstract—Aligning partially overlapping point sets where there is no prior information about the value of the transformation is a challenging problem in computer vision. To achieve this goal, we first reduce the objective of the robust point matching algorithm to a function of a low dimensional variable. The resulting function, however, is only concave over a finite region including the feasible region. To cope with this issue, we employ the inner approximation optimization algorithm which only operates within the region where the objective function is concave. Our algorithm does not need regularization on transformation, and thus can handle the situation where there is no prior information about the values of the transformations. Our method is also ϵ -globally optimal and thus is guaranteed to be robust. Moreover, its most computationally expensive subroutine is a linear assignment problem which can be efficiently solved. Experimental results demonstrate the better robustness of the proposed method over state-of-the-art algorithms. Our method is also efficient when the number of transformation parameters is small.

Index Terms—branch and bound, concave optimization, linear assignment, point correspondence, robust point matching

I. INTRODUCTION

Point matching is a fundamental problem in computer vision, pattern recognition and medical image analysis. Disturbances such as deformation, occlusion, outliers and noise often makes this problem challenging. One way of achieving point matching is through the optimization of the objective function of the robust point matching (RPM) algorithm [5]. By eliminating the transformation variable, the work of [14] reduces the objective function of RPM to a concave quadratic function of point correspondence with a low rank Hessian matrix. It then uses the normal rectangular algorithm, a variant of the branch-and-bound (BnB) algorithm, for optimization. But it requires that each model point has a counterpart in another point set, which limits the method's scope of applications.

To address this issue, the work of [13] reduces the objective function of RPM to a concave function of point correspondence, which, albeit not quadratic, still has a low rank structure. [13] then uses the normal simplex algorithm, a variant of the BnB algorithm, for optimization. However, [13] requires that the objective function is concave over a set of

simplexes whose union includes the feasible region, whereas the objective function is not necessarily concave outside the feasible region. To address this issue, it enlarges the concavity region of the objective function by adding a regularization on transformation where prior information about values of the transformation needs to be supplied. Consequently, the method tends to generate transformations biased towards the prior values. So the method may fail to handle the situation where prior information about the values of the transformations is unknown.

To address this issue, in this paper, we propose an alternative concave optimization approach. Instead of using the BnB algorithm which requires concavity of the objective function over a sufficiently large region, we use the inner approximation algorithm [10] which only operates within the region over which the objective function is concave. Thus, our method does not need regularization on transformation and is able to handle the situation that there is no prior information about the values of the transformation. Our method is also ϵ -globally optimal and thus is guaranteed to be robust. Moreover, its computationally expensive subroutine is a linear assignment problem which can be efficiently solved.

II. RELATED WORK

A. Heuristic based point matching methods

The methods related to ours are those modeling transformation and point correspondence. ICP [2], [22] iterates between estimating point correspondence and updating transformation. But it is prone to be trapped in local minima due to discrete nature of point correspondence. RPM [5] relaxes point correspondence to be fuzzily valued and uses deterministic annealing (DA) for optimization. But DA is biased towards matching the mass centers of two point sets.

The second category of methods are those modeling only transformation. The CPD method [16] casts point matching as the problem of fitting a Gaussian Mixture Model (GMM) representing one point set to another point set. The GMMREG method [11] uses GMMs to represent two point sets and minimizes the L_2 distance between them. The Schrödinger distance transform is used to represent point sets in [6] and the registration problem is converted into that of computing the geodesic distance between two points on a unit Hilbert sphere. Support vector parameterized Gaussian mixtures (SVGMS) has been proposed in [3] to represent point sets using sparse Gaussian components. The efficiency of GMM based methods is improved by using filtering to solve the correspondence problem in [8].

W. Lian is with the Department of Computer Science, Changzhi University, Changzhi, 046011, Shanxi, China, and the Department of Computing, The Hong Kong Polytechnic University, Hong Kong. E-mail: lianwei3@gmail.com.

W.-M. Zuo is with School of Computer Science and Technology, Harbin Institute of Technology (HIT), Harbin, China. E-mail: cswmzuo@gmail.com.

L. Zhang is with the Department of Computing, The Hong Kong Polytechnic University, Hung Hom, Kowloon, Hong Kong. E-mail: cslzhang@comp.polyu.edu.hk.

The above methods are all heuristic schemes. Therefore, they may not perform well when the point matching problem becomes difficult.

B. Global optimization-based methods

The branch-and-bound (BnB) algorithm is a popular global optimization technique. It is used to align 3D shapes based on the Lipschitz optimization theory [12]. But the method assumes no occlusion or outliers. BnB is used to recover 3D rigid transformation in [17]. But the correspondence needs to be known a priori. The Go-ICP method [21] uses BnB to optimize the ICP objective by exploiting the structure of the geometry of 3D rigid motions. The fast rotation search (FRS) method [1], [18] recovers rotation between 3D point sets by using stereographic projections. The general 6 degree rigid registration is accomplished by using a nested BnB algorithm. The GOGMA method registers two point sets by aligning the GMMs constructed from the original point sets [4]. Liu *et al.* proposed a rotation-invariant feature in [15]. Straub *et al.* proposed a novel way of tessellating rotation space in [19]. The above methods are all targeted at rigid registration. Therefore, they may not cope well with scaling and non-rigid deformation.

III. REFORMULATION OF OBJECTIVE FUNCTION

In this section, we mainly follow the work of [13] to derive our objective function. Suppose there are two point sets $\mathcal{X} = \{\mathbf{x}_i, i = 1, \dots, n_x\}$ and $\mathcal{Y} = \{\mathbf{y}_j, j = 1, \dots, n_y\}$ in \mathbb{R}^{n_d} to be matched, where the coordinates $\mathbf{x}_i = [x_i^1, \dots, x_i^{n_d}]^\top$ and $\mathbf{y}_j = [y_j^1, \dots, y_j^{n_d}]^\top$. RPM achieves point matching by essentially solving the following mixed linear assignment–least square problem:

$$\begin{aligned} \min E(\mathbf{P}, \boldsymbol{\varphi}) &= \sum_{i,j} p_{ij} \|\mathbf{y}_j - T(\mathbf{x}_i|\boldsymbol{\varphi})\|^2 \\ \text{s.t. } \mathbf{P}\mathbf{1}_{n_y} &\leq \mathbf{1}_{n_x}, \mathbf{1}_{n_x}^\top \mathbf{P} \leq \mathbf{1}_{n_y}^\top, \mathbf{1}_{n_x}^\top \mathbf{P}\mathbf{1}_{n_y} = n_p, \mathbf{P} \geq 0 \end{aligned} \quad (1)$$

$$(2)$$

where $T(\mathbf{x}_i|\boldsymbol{\varphi})$ denotes a transformation with parameters $\boldsymbol{\varphi}$. \mathbf{P} denotes a correspondence matrix with element $p_{ij} = 1$ indicating that there is a matching between \mathbf{x}_i and \mathbf{y}_j and $p_{ij} = 0$ otherwise. $\mathbf{1}_{n_x}^\top \mathbf{P}\mathbf{1}_{n_y} = n_p$ means the number of matches is equal to n_p , a preset positive integer.

Under the condition that $T(\mathbf{x}_i|\boldsymbol{\varphi})$ is linear w.r.t. its parameters $\boldsymbol{\varphi}$, i.e., $T(\mathbf{x}_i|\boldsymbol{\varphi}) = \mathbf{J}(\mathbf{x}_i)\boldsymbol{\varphi}$, where $\mathbf{J}(\mathbf{x}_i)$ is called the Jacobian matrix, after eliminating $\boldsymbol{\varphi}$ via solving $\frac{\partial E}{\partial \boldsymbol{\varphi}} = 0$ for $\boldsymbol{\varphi}$ and making substitution, the objective function can be written as:

$$\begin{aligned} E(\mathbf{P}) &= \mathbf{1}_{n_x}^\top \mathbf{P}\tilde{\mathbf{y}} \\ &- \mathbf{y}^\top (\mathbf{P} \otimes \mathbf{I}_{n_d})^\top \mathbf{J}(\mathbf{J}^\top (\text{diag}(\mathbf{P}\mathbf{1}_{n_y}) \otimes \mathbf{I}_{n_d})\mathbf{J})^{-1} \mathbf{J}^\top (\mathbf{P} \otimes \mathbf{I}_{n_d})\mathbf{y} \end{aligned} \quad (3)$$

where the matrix $\mathbf{J} \triangleq [\mathbf{J}^\top(\mathbf{x}_1), \dots, \mathbf{J}^\top(\mathbf{x}_{n_x})]^\top$ and the vectors $\mathbf{y} \triangleq [\mathbf{y}_1^\top, \dots, \mathbf{y}_{n_y}^\top]^\top$, $\tilde{\mathbf{y}} \triangleq [\|\mathbf{y}_1\|_2^2, \dots, \|\mathbf{y}_{n_y}\|_2^2]^\top$. $\mathbf{1}_{n_x}$ denotes the n_x -dimensional vector of all ones and \mathbf{I}_{n_d} denotes the n_d -dimensional identity matrix.

To facilitate optimization of E , P needs to be vectorized. We define the vectorization of a matrix as the concatenation of its rows, denoted by $\text{vec}(\cdot)$. Let $\mathbf{p} \triangleq \text{vec}(\mathbf{P})$. To obtain a concise form of E , we need to introduce new denotations. Let

$$\mathbf{1}_{n_x}^\top \mathbf{P}\tilde{\mathbf{y}} = \boldsymbol{\rho}^\top \mathbf{p}, \quad \mathbf{J}^\top (\mathbf{P} \otimes \mathbf{I}_{n_d})\mathbf{y} = \boldsymbol{\Gamma}\mathbf{p}, \quad (4)$$

$$\text{vec}(\mathbf{J}^\top (\text{diag}(\mathbf{P}\mathbf{1}_{n_y}) \otimes \mathbf{I}_{n_d})\mathbf{J}) = \text{vec}(\mathbf{J}_2^\top ((\mathbf{P}\mathbf{1}_{n_y}) \otimes \mathbf{I}_{n_\varphi})) = \boldsymbol{\Xi}\mathbf{p} \quad (5)$$

where n_φ denotes the dimension of $\boldsymbol{\varphi}$ and $\mathbf{J}_2 \triangleq [\mathbf{J}(\mathbf{x}_1)^\top \mathbf{J}(\mathbf{x}_1), \dots, \mathbf{J}(\mathbf{x}_{n_x})^\top \mathbf{J}(\mathbf{x}_{n_x})]^\top$. Based on the fact that $\text{vec}(\mathbf{M}_1\mathbf{M}_2\mathbf{M}_3) = (\mathbf{M}_1 \otimes \mathbf{M}_3)^\top \text{vec}(\mathbf{M}_2)$ for any multiplicable matrices \mathbf{M}_1 , \mathbf{M}_2 and \mathbf{M}_3 , we have

$$\boldsymbol{\rho} = \mathbf{1}_{n_x} \otimes \tilde{\mathbf{y}}, \quad \boldsymbol{\Gamma} = (\mathbf{J}^\top \otimes \mathbf{y}^\top) \mathbf{W}_{n_d, n_y}^{n_x, n_y}, \quad (6)$$

$$\boldsymbol{\Xi} = (\mathbf{J}_2^\top \otimes \mathbf{I}_{n_\varphi}) \mathbf{W}_{n_\varphi}^{n_x, 1} (\mathbf{I}_{n_x} \otimes \mathbf{1}_{n_y}^\top) \quad (7)$$

Please refer to [13] for definition of the constant matrix $\mathbf{W}_{n_d, n_y}^{n_x, n_y}$.

With the above preparation, E can be rewritten in terms of vector \mathbf{p} as:

$$E(\mathbf{p}) = \boldsymbol{\rho}^\top \mathbf{p} - \mathbf{p}^\top \boldsymbol{\Gamma}^\top \text{mat}(\boldsymbol{\Xi}\mathbf{p})^{-1} \boldsymbol{\Gamma}\mathbf{p} \quad (8)$$

where $\text{mat}(\cdot)$ denotes reconstructing a symmetric matrix from a vector which is the result of applying $\text{vec}(\cdot)$ to a symmetric matrix. Thus, $\text{mat}(\cdot)$ can be viewed as the inverse of the operator $\text{vec}(\cdot)$.

Since $\mathbf{1}_{n_x n_y}^\top \mathbf{p} = n_p$, a constant, rows in $\boldsymbol{\Xi}$ equal to scaled versions of $\mathbf{1}_{n_x n_y}^\top$ will be useless and can be discarded. Also, redundant rows can be removed. Since $\text{mat}(\boldsymbol{\Xi}\mathbf{p})$ is a symmetric matrix, $\boldsymbol{\Xi}$ contains redundant rows. Based on this analysis, we hereby denote $\boldsymbol{\Xi}_2$ as the matrix formed as a result of $\boldsymbol{\Xi}$ removing such rows. Please refer to Section V for examples of $\boldsymbol{\Xi}_2$. In view of the form of E , we can see that E is determined by the variable $[\boldsymbol{\Xi}_2^\top, \boldsymbol{\Gamma}^\top, \boldsymbol{\rho}]^\top \mathbf{p} = \mathbf{R}^\top \mathbf{Q}^\top \mathbf{p}$, which in turn is determined by a low dimensional variable $\mathbf{u}' \triangleq \mathbf{Q}^\top \mathbf{p}$. Here $\mathbf{Q}\mathbf{R}$ denotes the QR factorization of $[\boldsymbol{\Xi}_2^\top, \boldsymbol{\Gamma}^\top, \boldsymbol{\rho}]$ with \mathbf{R} being an upper triangular matrix and the columns of \mathbf{Q} being orthogonal unity vectors. The specific form of E in terms of variable \mathbf{u}' is:

$$E(\mathbf{u}') = (\mathbf{R}^\top \mathbf{u}')_\rho - (\mathbf{u}'^\top \mathbf{R})_\Gamma [\text{mat}((\mathbf{R}^\top \mathbf{u}')_{\boldsymbol{\Xi}_2})^{-1} (\mathbf{R}^\top \mathbf{u}')_\Gamma] \quad (9)$$

where $(\mathbf{R}^\top \mathbf{u}')_{\boldsymbol{\Xi}_2}$ denotes the vector formed by the elements of vector $\mathbf{R}^\top \mathbf{u}'$ with indices equal to row indices of the submatrix $\boldsymbol{\Xi}_2$ in matrix $[\boldsymbol{\Xi}_2^\top, \boldsymbol{\Gamma}^\top, \boldsymbol{\rho}]^\top$. Vectors $(\mathbf{R}^\top \mathbf{u}')_\Gamma$ and $(\mathbf{R}^\top \mathbf{u}')_\rho$ are similarly defined. Here we abuse the use of 'mat' such that $\text{mat}(\boldsymbol{\Xi}_2\mathbf{p}) = \text{mat}(\boldsymbol{\Xi}\mathbf{p})$. The meaning will be clear from the context.

IV. OPTIMIZATION

The analysis in the previous section indicates that E is a function of the low dimensional variable \mathbf{u}' with the feasible region $U' \triangleq \{\mathbf{u}' : \mathbf{u}' = \mathbf{Q}^\top \mathbf{p}, \mathbf{p} \in \Omega\}$, where Ω denotes the feasible region of \mathbf{p} , as is defined by (2).

Based on Proposition 1 in [13], one can see that E is concave over the spectrahedra $\Psi' \triangleq \{\mathbf{u}' : \text{mat}((\mathbf{R}^\top \mathbf{u}')_{\boldsymbol{\Xi}_2}) \succ 0\} \supset U'$. Thus, it is natural to use the inner approximation

algorithm [10], a global optimization algorithm specifically designed for functions which are concave over a finite region, to optimize E .

A. Translation of the coordinate system

To facilitate further derivation, it is convenient to work in a new coordinate system which is constructed as follows.

We first solve a series of linear assignment problems

$$\max\{\mathbf{h}_i^\top \mathbf{u}' : \mathbf{u}' \in U'\}, \quad (10)$$

to obtain $n_u + 1$ solutions $\mathbf{v}'_i \in U'$. Here n_u denotes the dimension of \mathbf{u}' and $\mathbf{h}_i, i = 1, \dots, n_u + 1$ are preset n_u -dimensional vectors such that $\mathbf{h}_i - \mathbf{h}_{n_u+1}$ are linearly independent. Different choices of \mathbf{h}_i are possible. For simplicity, in this paper, we choose \mathbf{h}_i as $\mathbf{e}_i, i = 1, \dots, n_u$ and $-\mathbf{1}_{n_u}$, respectively. Here \mathbf{e}_i denotes the n_u -dimensional vector with the i -th element being 1 and remaining elements being 0s. Let $\mathbf{v}'_0 = \frac{1}{n_u} \sum_i \mathbf{v}'_i$. Apparently, $\mathbf{v}'_0 \in \text{int}S'$, where "int" denotes the interior of a convex set and the simplex $S' \triangleq \text{co}\{\mathbf{v}'_1, \dots, \mathbf{v}'_{n_u+1}\} \subset U'$. Here $\text{co}\{\}$ denotes the convex hull of a point set.

Now we define the new coordinate system as the result of translating the coordinate system of \mathbf{u}' such that \mathbf{v}'_0 is the new origin. Points \mathbf{u} and \mathbf{u}' in the new and old coordinate systems are related by $\mathbf{u}' = \mathbf{u} + \mathbf{v}'_0$. Accordingly, the energy function for \mathbf{u} is $E_2(\mathbf{u}) \triangleq E(\mathbf{u} + \mathbf{v}'_0) = E(\mathbf{u}')$. Besides, the feasible region of \mathbf{u} is $U \triangleq \{\mathbf{u} : \mathbf{u} = \mathbf{Q}^\top \mathbf{p} - \mathbf{v}'_0, \mathbf{p} \in \Omega\}$ and $E_2(\mathbf{u})$ is concave over the spectrahedra $\Psi \triangleq \{\mathbf{u} : \text{mat}((\mathbf{R}^\top(\mathbf{u} + \mathbf{v}'_0))_{\Xi_2}) \succ 0\}$. Let the simplex $S \triangleq \text{co}\{\mathbf{v}_1, \dots, \mathbf{v}_{n_u+1}\}$, where the vertices $\mathbf{v}_i = \mathbf{v}'_i - \mathbf{v}'_0$.

It is noted that, instead of using a vertex of the feasible region U' as the center of the new coordinate system in [10], we use an interior point of U' as the center of the new coordinate system. This brings the benefit that the facet enumeration procedure as will be presented in Section IV-G can be simplified.

B. The inner approximation algorithm

The basic idea of the inner approximation algorithm applied to our problem is as follows:

Construct a sequence of polytopes (i.e., bounded polyhedrons) D_1, D_2, \dots such that

- 1) $\emptyset \neq D_k \cap U \subset D_{k+1} \cap U$ and $D_k \subset \Psi$ for $k \geq 1$.
- 2) an optimal solution ω_1 of $\min\{E_2(\mathbf{u}) : \mathbf{u} \in D_1 \cap U\}$ is available.
- 3) an optimal solution ω_{k+1} of $\min\{E_2(\mathbf{u}) : \mathbf{u} \in D_{k+1} \cap U\}$ can be derived from an optimal solution ω_k of $\min\{E_2(\mathbf{u}) : \mathbf{u} \in D_k \cap U\}$.

The procedure stops when $D_k \supseteq U$, since, in this case, ω_k is an optimal solution of $\min\{E_2(\mathbf{u}) : \mathbf{u} \in U\}$. The sequence $U \cap D_1, U \cap D_2, \dots$ constitutes an inner approximation of U by "expanding" polytopes. The polytope D_{k+1} can be constructed from D_k by choosing a suitable point $\tilde{\mathbf{z}}_k \notin D_k$ and setting

$$D_{k+1} = \text{co}\{D_k \cup \{\tilde{\mathbf{z}}_k\}\} \quad (11)$$

To ensure convergence of the algorithm in finite iterations, we require that $D_{k+1} \setminus D_k$ contains a vertex of U . Therefore,

in each iteration, the algorithm finds a vertex \mathbf{z} of U satisfying $\mathbf{z} \notin D_k$, and determines $\tilde{\mathbf{z}}_k$ in (11) from \mathbf{z}_k such that

$$D_{k+1} = \text{co}(D_k \cup \{\tilde{\mathbf{z}}_k\}) \supseteq \text{co}(D_k \cup \{\mathbf{z}_k\}) \quad (12)$$

Usually $\tilde{\mathbf{z}}_k \neq \mathbf{z}_k$, thus, D_{k+1} will be strictly larger than $\text{co}(D_k \cup \{\mathbf{z}_k\})$. The purpose of using $\tilde{\mathbf{z}}_k$ instead of \mathbf{z}_k is to make D_{k+1} as large as possible so as to improve the convergence of the algorithm.

C. Initial polytope

Although the simplex $S = \text{co}\{\mathbf{v}_1, \dots, \mathbf{v}_{n_u+1}\}$ in Section IV-A can be used as the initial polytope, it is advantageous that the initial polytope is chosen as large as possible so as to improve the convergence of our algorithm. To this end, We next expand S by using a simplified version of the γ -extension [10] where we only specify directions.

Definition 1: A point $\tilde{\mathbf{d}}$ is called γ -extension in direction $\mathbf{d} \in \mathbb{R}^{n_u} \setminus \{0\}$ if

$$\tilde{\mathbf{d}} = \theta \mathbf{d} \quad \text{with} \quad \theta = \max\{t : E_2(t\mathbf{d}) \geq \gamma, t\mathbf{d} \in \Psi\}$$

We solve this problem by first solving the subproblem

$$\max\{t : t\mathbf{d} \in \Psi\} \quad (13)$$

This is a semidefinite program, for which solvers such as Sedumi [20] can be employed. Suppose the optimal t is t_0 , then we can use, e.g., the bisection algorithm to solve the second subproblem:

$$\max\{t : E_2(t\mathbf{d}) \geq \gamma, 0 \leq t \leq t_0\} \quad (14)$$

Let $\tilde{\mathbf{v}}_i = \theta_i \mathbf{v}_i$ be the γ -extension in direction \mathbf{v}_i with $\gamma = E_2(\boldsymbol{\omega})$. Here $\boldsymbol{\omega} = \arg \min_i E_2(\mathbf{v}_i)$ is the initial optimal solution. Due to concavity of E_2 over Ψ , it follows that $\theta_i \geq 1$. The unique hyperplane passing through $\tilde{\mathbf{v}}_i, i = 1, \dots, j-1, j+1, \dots, n_u + 1$ is

$$H^j = \{\mathbf{u} : \mathbf{u} = \mathbf{Y}_j \boldsymbol{\lambda}, \mathbf{1}_{n_u}^\top \boldsymbol{\lambda} = 1\} = \{\mathbf{u} : \mathbf{1}_{n_u}^\top \mathbf{Y}_j^{-1} \mathbf{u} = 1\} \quad (15)$$

where the matrix $\mathbf{Y}_j = [\tilde{\mathbf{v}}_1 \ \dots \ \tilde{\mathbf{v}}_{j-1} \ \tilde{\mathbf{v}}_{j+1} \ \dots \ \tilde{\mathbf{v}}_{n_u+1}]$. Since the origin $\mathbf{0} \in \text{int}S$, it follows that $\mathbf{v}_1, \dots, \mathbf{v}_{j-1}, \mathbf{v}_{j+1}, \dots, \mathbf{v}_{n_u+1}$ are linearly dependent, so do $\tilde{\mathbf{v}}_1, \dots, \tilde{\mathbf{v}}_{j-1}, \tilde{\mathbf{v}}_{j+1}, \dots, \tilde{\mathbf{v}}_{n_u+1}$. Thus, \mathbf{Y}_j is invertible. We define the half space $H_-^j \triangleq \{\mathbf{u} : \mathbf{1}_{n_u}^\top \mathbf{Y}_j^{-1} \mathbf{u} \leq 1\}$. Apparently, $\mathbf{0} \in \text{int}H_-^j$. We now set the initial polytope as the simplex

$$D = \cap_j H_-^j \quad (16)$$

Thus, $\mathbf{0} \in \text{int}D$.

D. Updating polytope

At some stage of the algorithm, we have

$$D = \{\mathbf{u} : \mathbf{d}_i^\top \mathbf{u} \leq 1, i \in I\} \quad (17)$$

with some finite index set I and $\tilde{\mathbf{z}} \in \mathbb{R}^{n_u} \setminus D$. Then the next polytope

$$\bar{D} = \text{co}(D \cup \{\tilde{\mathbf{z}}\}) \quad (18)$$

is of the form

$$\bar{D} = \{\mathbf{u} : \bar{\mathbf{d}}_i^\top \mathbf{u} \leq 1, i \in \bar{I}\} \quad (19)$$

Finding $\bar{\mathbf{d}}_i$ is a classical facet enumeration problem which will be treated in Section IV-G.

E. Termination condition

As shown in Section IV-B, the algorithm will terminate if $U \setminus D = \emptyset$. Since D is of the form (17), we can check whether $U \setminus D = \emptyset$ by solving the following linear assignment programs

$$\mu_i = \max\{\mathbf{d}_i^\top \mathbf{u} : \mathbf{u} \in U\} \quad (i \in I) \quad (20)$$

Then $Q = \{\mathbf{u} : \mathbf{d}_i^\top \mathbf{u} \leq \mu_i, i \in I\}$ is a polytope containing U , and we have $U \setminus D = \emptyset$ if and only if $D \supseteq Q$, i.e., if and only if $\mu_i \leq 1$ for each $i \in I$.

In this paper, instead of using the termination condition $\max_i \mu_i \leq 1$, which is generally computationally expensive, we set the termination criterion as $\max_j \mu_j \leq 1 + \epsilon$, where ϵ is a preset small positive value. Consequently, our algorithm becomes an ϵ -globally optimal algorithm. Since higher dimensional space of \mathbf{u} tends to lead to slower convergence, instead of directly setting ϵ , we let $\epsilon = n_u \epsilon_0$ by also taking into account the dimension n_u of the space of \mathbf{u} and set ϵ_0 instead.

F. Expanding polytope

If $\max_i \mu_i > 1 + \epsilon$, then we need to expand the polytope D . For $j^* = \arg \max_i \mu_i$, we have an optimal vertex solution $\mathbf{z} \in V(U) \setminus D$ of $\max\{\mathbf{d}_{j^*}^\top \mathbf{u} : \mathbf{u} \in U\}$. Here $V(\cdot)$ denotes the vertex set of a polytope.

As is shown before, a larger D benefits the convergence of our algorithm. To this end, we choose $\tilde{\mathbf{z}} = \theta \mathbf{z}$ as the γ -extension in direction \mathbf{z} with $\gamma = \min\{E_2(\mathbf{z}), E_2(\omega)\}$. Due to concavity of E_2 over Ψ , we have $\theta \geq 1$. We now set $\bar{D} = \text{co}(D \cup \{\tilde{\mathbf{z}}\})$. Meanwhile, the optimal solution so far obtained is updated as $\omega \leftarrow \arg \min\{E_2(\mathbf{z}), E_2(\omega)\}$.

G. Facet enumeration

Facet enumeration (FE) problem: Given a polytope D of the form (17) and given a point $\tilde{\mathbf{z}} \in \mathbb{R}^{n_u} \setminus D$, problem FE aims to find the inequality representation of $\bar{D} = \text{co}(D \cup \{\tilde{\mathbf{z}}\})$.

Instead of directly solving problem FE which is challenging, following [10], we use the concept of polars to equivalently transform this problem into the vertex enumeration problem (VE) and then solve the resulting problem.

Definition 2: Let $D \subset \mathbb{R}^{n_u}$ be a convex set. Then the set

$$D^0 = \{\mathbf{v} : \mathbf{v}^\top \mathbf{u} \leq 1 \text{ for all } \mathbf{u} \in D\} \quad (21)$$

is called the polar of D .

Geometrically speaking, the polar D^0 describes the set of normals to the hyperplanes $\{\mathbf{u} : \mathbf{v}^\top \mathbf{u} = 1\}$ such that the half spaces $\{\mathbf{u} : \mathbf{v}^\top \mathbf{u} \leq 1\}$ contain D . It is easy to see that D^0 is bounded if and only if the origin $\mathbf{0} \in \text{int}D$.

Theorem 1: (vertex-facet duality) Let $D = \{\mathbf{u} : \mathbf{d}_i^\top \mathbf{u} \leq 1, i \in I\}$, $\mathbf{d}_i \in \mathbb{R}^{n_u} \setminus \{\mathbf{0}\}, i \in I$ be a polytope whose facets

are defined by \mathbf{d}_i , and let D^0 be the polar of D with vertex set $V(D^0)$. Then

$$V(D^0) = \{\mathbf{d}_i : i \in I\} \quad (22)$$

Please refer to [10] for the proof. Note that compared with the corresponding theorem in [10], Theorem 1 has a simpler form without considering the extreme directions of D^0 . This is because for our algorithm, we have $\mathbf{0} \in \text{int}D$ and thus D^0 is bounded.

Returning to problem FE, we see from Theorem 1 that, when switching to polars, this problem is equivalent to a vertex enumeration (VE) problem, as is explained in the following corollary:

Corollary 1: Let D^0 and $\bar{D}^0 = D^0 \cap \{\mathbf{u} : \mathbf{u}^\top \tilde{\mathbf{z}} \leq 1\}$ be the polars of D and $\bar{D} = \text{co}(D \cup \{\tilde{\mathbf{z}}\})$, respectively, then each facet $\bar{D} \cap \{\mathbf{u} : \bar{\mathbf{d}}_i^\top \mathbf{u} = 1\}$ of \bar{D} corresponds to a vertex $\bar{\mathbf{d}}_i$ of \bar{D}^0 and vice versa.

Given $V(D^0)$, finding $V(\bar{D}^0)$ is precisely the classical problem of VE [10], which will be reviewed in the next section.

H. Vertex enumeration

Vertex Enumeration (VE) Problem: Let $D = \{\mathbf{u} : g_i(\mathbf{u}) = a_i^\top \mathbf{u} - b_i \leq 0, i = 1, \dots, m\}$ be a polytope with known vertex set $V(D)$, and let $H = \{\mathbf{u} : g_{m+1}(\mathbf{u}) = a_{m+1}^\top \mathbf{u} - b_{m+1} = 0\}$ be a hyperplane such that $\bar{D} = D \cap H$ is neither empty nor a facet of D . Problem VE aims to determine the vertex set $V(\bar{D})$ of \bar{D} .

Let

$$V^+(D) = \{\mathbf{v} \in V(D) : g_{m+1}(\mathbf{v}) > 0\} \quad (23)$$

$$V^-(D) = \{\mathbf{v} \in V(D) : g_{m+1}(\mathbf{v}) < 0\} \quad (24)$$

Without loss of generality, we assume $|V^-| \leq |V^+|$. Here $|\cdot|$ denotes the cardinality of a set. For each $\mathbf{u} \in V^-$, denote by $\mathcal{J}(\mathbf{u})$ the set of constraints of D which are active at \mathbf{u} . Because of the way D is constructed, vertex \mathbf{u} is nondegenerate, thus, we have $|\mathcal{J}(\mathbf{u})| = n_u$ and linear independence of the corresponding system of linear equations

$$a_i^\top \mathbf{u} - b_i = 0 \quad (i \in \mathcal{J}(\mathbf{u})) \quad (25)$$

Moreover, \mathbf{u} has n_u neighboring vertices in D . That is, n_u edges of D are incident with \mathbf{u} . Each line through \mathbf{u} in the direction of such an edge is the solution set of a system of $n_u - 1$ linear equations which can be obtained from (25) by dropping one equation. The set of new vertices in $D \cap H$ which are adjacent to \mathbf{u} contains the intersection points of these lines with the hyperplane H .

Without loss of generality, for simplicity of notation, we assume $\mathcal{J}(\mathbf{u}) = \{1, \dots, n_u\}$. Then, for each $\mathbf{u} \in V^-$, we have to consider the n_u systems of n_u linear equations

$$\begin{aligned} a_i^\top \mathbf{u} - b_i &= 0 \quad (i \in \{1, \dots, n_u\} \setminus \{l\}) \\ a_{m+1}^\top \mathbf{u} - b_{m+1} &= 0 \end{aligned} \quad (26)$$

which arise when l runs from 1 to n .

When a system in (26) has a solution ω , we have to check whether ω satisfies the remaining inequalities of D .

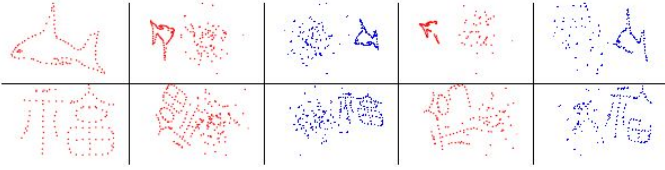


Fig. 1. Left column: the prototype shapes. For the remaining columns: examples of model and scene point sets in the outlier (columns 2, 3) and occlusion + outlier (columns 4, 5) tests.

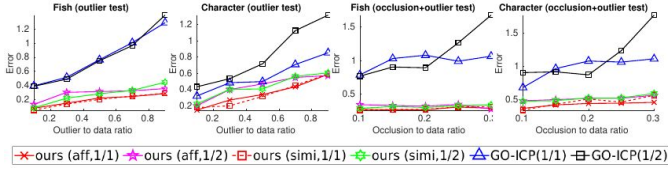


Fig. 2. Average matching errors by our method and Go-ICP with different n_p values (chosen from 1/2 to 1/1 the ground truth value) over 100 random trials for the 2D outlier and occlusion+outlier tests.

Instead of directly solving (26), which is cumbersome, in the following, the simplex pivoting algorithm is employed to solve this problem. It works by introducing slack variables $\mathbf{v} \in R_+^{n_u}$ to write the binding inequalities of $J(\mathbf{u})$ in the form

$$A\mathbf{u} + I_{n_u}\mathbf{v} = \mathbf{b} \quad (27)$$

and the equation of H in the form

$$a_{m+1}^\top \mathbf{u} + 0^\top \mathbf{v} = b_{m+1} \quad (28)$$

One can transform (27) into

$$I_{n_u}\mathbf{u} + A^{-1}\mathbf{v} = A^{-1}\mathbf{b} \quad (29)$$

and transform (28) (by adding to (28) multiples of the rows of (27)) into

$$0^T \mathbf{u} + \bar{a}^\top \mathbf{v} = \bar{b} \quad (30)$$

from which all possible new vertices neighboring \mathbf{u} can be obtained by pivoting on all the current nonbasic variables \mathbf{v} in the row (30).

V. EXPERIMENTS

We implement our method under Matlab 2019b and compare it with other methods on a PC with 3 GHz CPU and 32G RAM. For the competing methods which only output point correspondences, the generated correspondences are used to find the best affine transformations between two point sets. We define error as the root mean squared difference between the coordinates of transformed ground truth model inliers and those of their corresponding scene inliers. For our algorithm, we set the parameter $\epsilon_0 = 0.3$.

A. 2D synthesized datasets

We compare our method with Go-ICP [21], a globally optimal point set registration algorithm. Go-ICP can handle partial overlapping point sets and allows arbitrary rotation and translation between two point sets.

2D similarity and affine transformations are respectively considered for our method. For the former, we have the formulation of the transformation

$$T(\mathbf{x}_i|\varphi) = [\varphi_1 x_i^1 - \varphi_2 x_i^2 + \varphi_3, \quad \varphi_2 x_i^1 + \varphi_1 x_i^2 + \varphi_4]^\top \quad (31)$$

where $\varphi = [\varphi_1, \dots, \varphi_4]^\top$. Then we have the Jacobian matrix $\mathbf{J}(\mathbf{x}_i) = \begin{bmatrix} x_i^1 & -x_i^2 & 1 & 0 \\ x_i^2 & x_i^1 & 0 & 1 \end{bmatrix}$. It can be verified that the rows of $\Xi_2 = \Xi([1, 3, 4], :)$ constitute the unique rows of Ξ not equal to scaled versions of $\mathbf{1}_{n_x n_y}^\top$.

For 2D affine transformation, we have the formulation of the transformation

$$T(\mathbf{x}_i|\varphi) = [\varphi_1 x_i^1 + \varphi_2 x_i^2 + \varphi_5, \quad \varphi_3 x_i^1 + \varphi_4 x_i^2 + \varphi_6]^\top \quad (32)$$

where $\varphi = [\varphi_1, \dots, \varphi_6]^\top$. Then we have $\mathbf{J}(\mathbf{x}_i) = \begin{bmatrix} x_i^1 & x_i^2 & 0 & 0 & 1 & 0 \\ 0 & 0 & x_i^1 & x_i^2 & 0 & 1 \end{bmatrix}$. It can be verified that the rows of $\Xi_2 = \Xi([1, 2, 5, 8, 11], :)$ constitute the unique rows of Ξ not equal to scaled versions of $\mathbf{1}_{n_x n_y}^\top$.

Following [13], two categories of tests are conducted: 1) **Outlier test** and 2) **Occlusion + Outlier test**. Different from [13], disturbances of random rotation and scaling within range [0.5, 1.5] are also added when generating the model point sets. Fig. 1 illustrates these tests and the prototype shapes.

The matching errors by different methods are presented in Fig. 2. One can see that our method using either transformation performs better than Go-ICP, particularly in the occlusion+outlier test, where there is a large margin between the errors of our method and that of Go-ICP. In terms of different choices of transformations, our method using similarity or affine transformation performs similar to each other. In terms of different choices of n_p , our method with n_p close to the ground truth performs only slightly better. This demonstrates that our method is insensitive to different choices of n_p .

The average running times (in seconds) by different methods are: 8.45 or 467.46 for our method using similarity or affine transformation and 12.19 for Go-ICP. This demonstrates high efficiency of our method using similarity transformation. Our method using affine transformation is two orders of magnitude slower than our method using similarity transformation. This is because affine transformation has larger number of parameters.

B. 2D point sets extracted from images

Point sets extracted from images are a more realistic setting for testing algorithms. We test different methods on 2D point sets extracted via the Canny edge detector from several images in the Caltech-256 [9] and VOC2007 [7] datasets, as illustrated in Fig. 3. To test a method's ability at handling rotations, model point sets are rotated 180 degree before being matched to scene point sets.

The registration results by different methods are presented in Fig. 3. One can see that our method using similarity transformation performs the best, while Go-ICP and our method using affine transformation performs not well. This is because affine transformation has more transformation freedom than rigid (which is used by Go-ICP) or similarity (which is used by

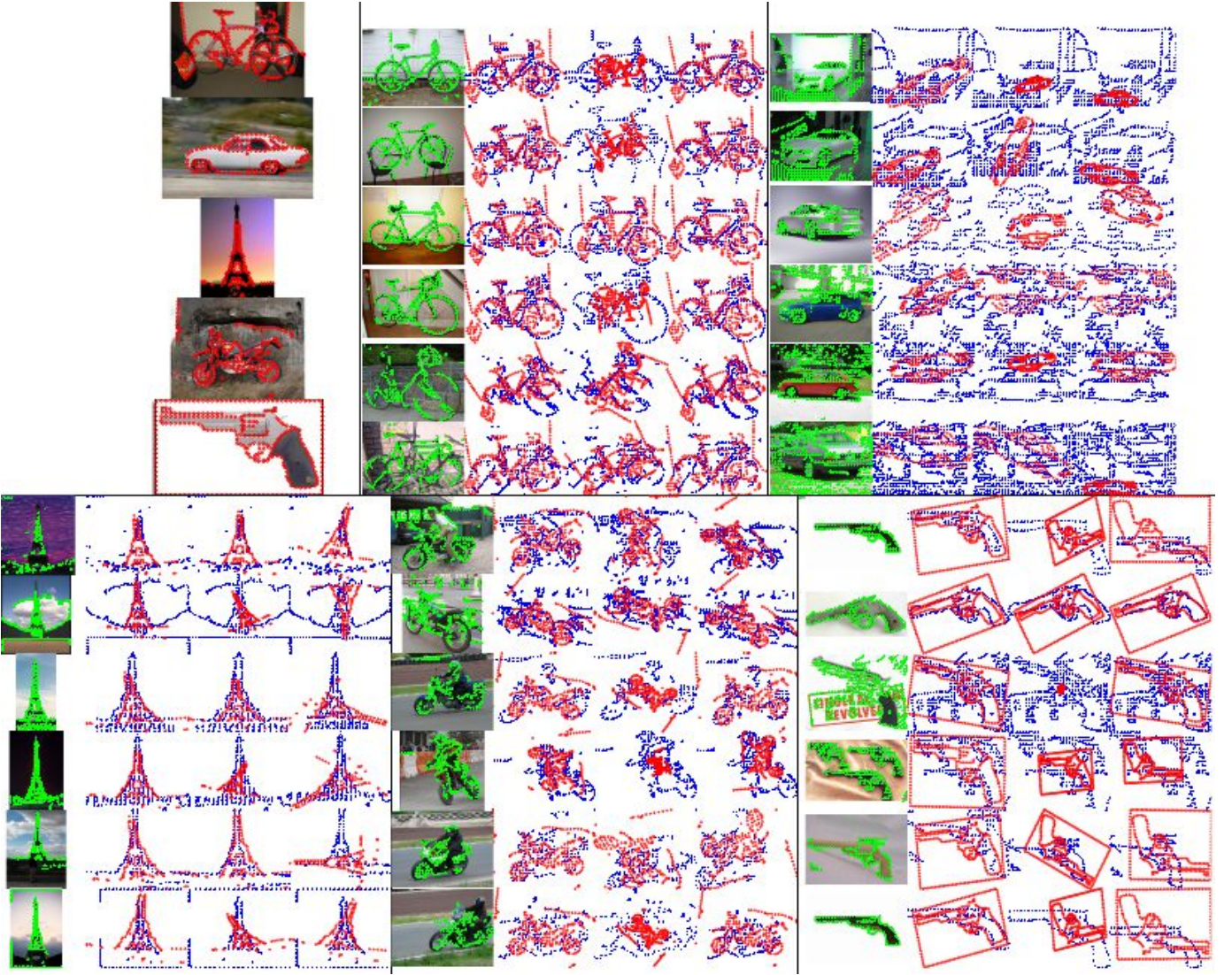


Fig. 3. Top left grid cell: model images with model point sets superimposed. The remaining cells: scene images with scene point sets superimposed, alignment results by our method using similarity or affine transformations and Go-ICP. The n_p value for every method is chosen as 0.9 the minimum of the cardinalities of two point sets.

another transformation version of our method) transformation, leading to the possibility of unconstrained registration results. Another factor is that for our method, the tolerance error $\epsilon = n_u \epsilon_0$ for affine transformation is actually larger than that of similarity transformation given that ϵ_0 is set the same for both types of transformations.

C. 3D synthesized datasets without rotations

Since 3D affine transformation contains many parameters which causes our method to converge too slowly, it will not be tested. Instead, We consider the 3D transformation consisting of nonuniform scaling and translation for our method:

$$T(\mathbf{x}_i|\boldsymbol{\varphi}) = [\varphi_1 x_i^1 + \varphi_4, \quad \varphi_2 x_i^2 + \varphi_5, \quad \varphi_3 x_i^3 + \varphi_6]^\top \quad (33)$$

where $\boldsymbol{\varphi} = [\varphi_1, \dots, \varphi_6]$. We have the Jacobian matrix $\mathbf{J}(\mathbf{x}_i) = \begin{bmatrix} x_i^1 & 0 & 0 & 1 & 0 & 0 \\ 0 & x_i^2 & 0 & 0 & 1 & 0 \\ 0 & 0 & x_i^3 & 0 & 0 & 1 \end{bmatrix}$. It can be verified that the

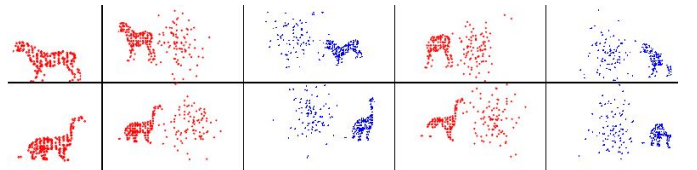


Fig. 4. Left column: the prototype shapes. For the remaining columns: examples of model and scene point sets in the outlier (columns 2, 3) and occlusion+outlier (columns 4, 5) tests.

rows of $\Xi_2 = \Xi([1, 4, 8, 11, 15, 18], :)$ constitute the unique rows of Ξ not equal to scaled versions of $\mathbf{1}_{mn}^\top$.

We compare our method with RPM-BnB [13], RPM [5], CPD [16] and GMMREG [11]. These methods only utilize the point position information for matching, and are capable of handling partial overlapping point sets. RPM-BnB is also globally optimal, making it a good candidate for comparison.

Analogous to the experimental setup in Section V-A, we

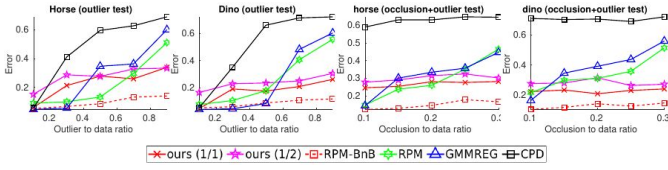


Fig. 5. Average matching errors by our method with different n_p values (chosen from 1/2 to 1/1 the ground truth value) and other methods over 100 random trials for the 3D outlier and occlusion+outlier tests.

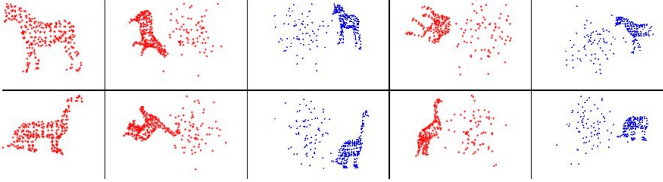


Fig. 6. Left column: the prototype shapes. For the remaining columns: examples of model and scene point sets in the outlier (columns 2, 3) and occlusion + outlier (columns 4, 5) tests.

conduct two categories of tests: 1) **Outlier test** and 2) **Occlusion + Outlier test**. Different from Section V-A, no rotation disturbance is added when generating the point sets. Fig. 4 illustrates these tests and the prototype shapes. The matching errors by different methods are presented in Fig. 5. One can see that our method performs slightly poorer than RPM-BnB. Nevertheless, it is as robust as RPM-BnB by performing the same with increase of severity of disturbance. Note that our method is more versatile (e.g., being able to handle 2D similarity invariant alignment problem) than RPM-BnB. In comparison, RPM, CPD and GMMREG only perform well when the disturbance is not severe. The result also indicates that our method is relatively insensitive to different choices of n_p .

The average running times (in seconds) by different methods are: 2769.5 for our method, 18.65 for RPM-BnB, 3.2 for RPM, 0.3 for GMMREG and 0.1 for CPD.

D. 3D synthesized datasets with rotations around z-axis

Next, we consider the 3D transformation consisting of rotation around z -axis, uniform scaling on the x - y plane, scaling along z -axis and translation for our method:

$$T(\mathbf{x}_i|\varphi) = [\varphi_1 x_i^1 - \varphi_2 x_i^2 + \varphi_4, \quad \varphi_2 x_i^1 + \varphi_1 x_i^2 + \varphi_5, \quad \varphi_3 x_i^3 + \varphi_6] \quad (34)$$

where $\varphi = [\varphi_1, \dots, \varphi_6]$. We have the Jacobian matrix $\mathbf{J}(\mathbf{x}_i) = \begin{bmatrix} x_i^1 & -x_i^2 & 0 & 1 & 0 & 0 \\ x_i^2 & x_i^1 & 0 & 0 & 1 & 0 \\ 0 & 0 & x_i^3 & 0 & 0 & 1 \end{bmatrix}$. It can be verified that the rows of $\Xi_2 = \Xi([1, 4, 5, 15, 18], :)$ constitute the unique rows of Ξ not equal to scaled versions of $\mathbf{1}_{mn}^\top$.

In this section, besides Go-ICP, we also compare with FRS [18], which is based on global optimization, only utilizes point coordinate information and allows arbitrary rotations and translations between two point sets.

Analogous to the experimental setup in Section V-C, we conduct two categories of tests: 1) **Outlier test** and 2) **Occlusion + Outlier test**. Different from Section V-C, random

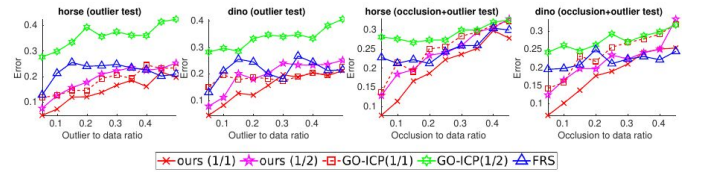


Fig. 7. Average matching errors by our method and Go-ICP with different n_p values (chosen from 1/2 to 1/1 the ground truth value) and FRS over 100 random trials for the 3D outlier and occlusion+outlier tests.

rotation around the z -axis and uniform scaling within range $[0.5, 1.5]$ is applied to the prototype shape when generating the model point sets. Fig. 6 illustrates these tests and the prototype shapes. The matching errors by different methods are presented in Fig. 7. One can see that our method performs overall better than other methods and is less sensitive to different choices of n_p than Go-ICP.

The average running time (in seconds) by different methods are: 177.73 for our method, 69.26 for Go-ICP and 268.96 for FRS.

VI. CONCLUSION

We proposed a global optimization-based algorithm for matching partially overlapping point sets. It works by reducing the RPM objective function to a function of a low dimensional variable and then using the inner approximation algorithm to optimize the resulting objective function over its concave region. Experiments on 2D and 3D data sets demonstrated better robustness of the proposed method over state-of-the-art algorithms for tasks involving various types of disturbances. It is also efficient when the number of transformation parameters is small.

ACKNOWLEDGMENTS

This work was supported by National Natural Science Foundation of China under Grant 61773002.

REFERENCES

- [1] J.-C. Bazin, Y. Seo, and M. Pollefeys. Globally optimal consensus set maximization through rotation search. In *Asian Conference on Computer Vision*, 2012.
- [2] P. J. Besl and N. D. McKay. A method for registration of 3-d shapes. *IEEE Trans. Pattern Analysis and Machine Intelligence*, 14(2):239–256, 1992.
- [3] D. Campbell and L. Petersson. An adaptive data representation for robust point-set registration and merging. In *ICCV*, 2015.
- [4] D. Campbell and L. Petersson. Gogma: Globally-optimal gaussian mixture alignment. In *The IEEE Conference on Computer Vision and Pattern Recognition*, June 2016.
- [5] H. Chui and A. Rangarajan. A new point matching algorithm for non-rigid registration. *Computer Vision and Image Understanding*, 89(2-3):114–141, 2003.
- [6] Y. Deng, A. Rangarajan, S. Eisenschenk, and B. C. Vemuri. A riemannian framework for matching point clouds represented by the schrödinger distance transform. In *IEEE Conference on Computer Vision and Pattern Recognition*, 2014.
- [7] M. Everingham, L. Van Gool, C. K. I. Williams, J. Winn, and A. Zisserman. The PASCAL Visual Object Classes Challenge 2007 (VOC2007) Results. <http://www.pascal-network.org/challenges/VOC/voc2007/workshop/index.html>.
- [8] W. Gao and R. Tedrake. Filterreg: Robust and efficient probabilistic point-set registration using gaussian filter and twist parameterization. In *CVPR*, 2019.

- [9] G. Griffin, A. Holub, and P. Perona. Caltech-256 object category dataset, 2007. technical report, California Inst. of Technology.
- [10] R. Horst, P. M. Pardalos, and N. V. Thoai. *Introduction to Global Optimization - Second Edition*. Springer, 2000.
- [11] B. Jian and B. C. Vemuri. Robust point set registration using gaussian mixture models. *IEEE Trans. Pattern Analysis and Machine Intelligence*, 33(8):1633–1645, 2011.
- [12] H. Li and R. Hartley. The 3d-3d registration problem revisited. In *International Conference on Computer Vision*, 2007.
- [13] W. Lian and L. Zhang. Point matching in the presence of outliers in both point sets: A concave optimization approach. In *IEEE Conference on Computer Vision and Pattern Recognition*, pages 352–359, 2014.
- [14] W. Lian, L. Zhang, and M.-H. Yang. An efficient globally optimal algorithm for asymmetric point matching. *IEEE Transactions on Pattern Analysis and Machine Intelligence*, 2016.
- [15] Y. Liu, C. Wang, Z. Song, and M. Wang. Efficient global point cloud registration by matching rotation invariant features through translation search. In *The European Conference on Computer Vision (ECCV)*.
- [16] A. Myronenko and X. Song. Point set registration: Coherent point drift. *IEEE Transactions on Pattern Analysis and Machine Intelligence*, 32(12):2262–2275, 2010.
- [17] C. Olsson, F. Kahl, and M. Oskarsson. Branch-and-bound methods for euclidean registration problems. *IEEE Transactions on Pattern Analysis and Machine Intelligence*, 31(5):783–794, 2009.
- [18] Á. Parra, T.-J. Chin, A. Eriksson, H. Li, and D. Suter. Fast rotation search with stereographic projections for 3d registration. *IEEE Transactions on Pattern Analysis and Machine Intelligence*, 38(11):2227–2240, 2016.
- [19] J. Straub, T. Campbell, J. P. How, and J. W. Fisher. Efficient global point cloud alignment using bayesian nonparametric mixtures. In *Proc. IEEE Conf. Comput. Vis. Pattern Recog.*, pages 2403–2412, 2017.
- [20] J. Sturm. Using sedumi 1.02, a matlab toolbox for optimization over symmetric cones. *Optimization Methods and Software*, pages 625–653, 1999.
- [21] J. Yang, H. Li, and Y. Jia. Go-icp: Solving 3d registration efficiently and globally optimally. In *International Conference on Computer Vision*, 2013.
- [22] Z. Zhang. Iterative point matching for registration of free-form curves and surfaces. *International Journal of Computer Vision*, 13(2):119–152, 1994.